Longitudinal ion-clearing mechanism in space-charge neutralization of low energy beams

C. A. Valerio-Lizarraga*

Facultad de Ciencias Físico-Matemáticas Universidad Autónoma de Sinaloa, Avenida de las Américas y Boulevard Universitarios S/N, Sinaloa, 80010, Mexico

(Received 8 August 2023; accepted 1 April 2024; published 20 May 2024)

In electron guns, generating high-intensity beams comes with the cost of increasing the number of secondary ions produced by the residual gas ionization which can be a limiting factor in the cathode lifetime. However, it is often overlooked that the longitudinal potential generated by the beam can be the main factor influencing secondary ions to drift back toward the source and limit the maximum beam intensity. Using 3D simulations, this paper shows how the flux of trapped ions depends on the beam parameters. The results provide a practical framework that can be used as a guide in the design of the electron gun focal point to mitigate the ion back bombardment.

DOI: 10.1103/PhysRevAccelBeams.27.050101

I. INTRODUCTION

One of the main limitations in generating high-intensity electron beams in direct current (dc) photoemission guns is the damage to the extraction system caused by secondary ion back bombardment, which restricts its maximum intensity operation and lifetime [1], requiring gun operation in extreme-high vacuum conditions [2]. Additional mitigation of the ion-back bombardment effect can be achieved by positively biasing the anode and utilizing asymmetric guns [3,4].

Positive ions and electrons are created through the interaction of the beam with residual gas in the beamline by ionization. In the case of negatively charged beams, if their energy is lower than the beam potential, positive ions trapped by the beam and secondary electrons are expelled radially. As the beam intensity increases, so does the number of secondary ions produced by the H_2 residual gas ionization, as defined by Eq. (1).

$$\frac{\partial n_{H_2}}{\partial t} = n_b n_{H_2} \sigma_i v_b = \frac{n_b}{\tau}. \tag{1}$$

Where σ_i is the ionization cross section, v_b the beam velocity, n_{H_2} and n_b the residual gas and beam density, respectively. The neutralization time is defined as $\tau = \frac{1}{n_{H_2}\sigma_{H_2} v_b}$.

Within the beamline, the secondary ions typically cause minimal surface damage upon colliding with the beam pipe. However, as they enter an acceleration region, these ions can gain sufficient energy to inflict notable surface damage, produce sputtering, and induce secondary electron emission [5].

Once the secondary ions are trapped by the beam (assuming no ion-clearing mechanisms and considering only the radial component), they oscillate around the beam center gradually accumulating, therefore inducing space-charge neutralization (SCN), and the electrostatic potential disappears, enabling ions to exit the system radially, establishing a steady-state solution where the local potential oscillates around zero [6–8].

The quantity of ions that the beam can trap depends on the potential well generated by the beam itself and the energy of the secondary ions. The neutralization time dictates when the system ultimately reaches this steady-state solution. The final electrostatic potential in the steady-state solution should be independent of the residual gas pressure in the beamline.

Previous studies involving measurements and simulations of a low-energy system [9,10] indicated that the beam potential is not fully neutralized once it reaches the steady state.

The discrepancy in the system can be caused by external electric fields generated by the source or accelerating cavities in the beamline. However, in scenarios where there are no external fields to clear ions radially (such as in a drift region), the under-neutralization in the beam should result from longitudinal losses within the system.

This work focuses on the influence of beam dynamics and external electric fields on ion-clearing mechanisms, consequently affecting the level of neutralization in the low-energy beam transport (LEBT). The simulations used in this work are performed using a modified version of the code IBsimu [11] which has previously been employed to

*cvalerio@uas.edu.mx

study beam neutralization and compared with measurements with good agreement [9,12].

II. ION LIFETIME UNDER BEAM POTENTIAL

The simplest scenario occurs when a nondivergent beam travels through a drift region without generating a longitudinal electric field. Once the secondary ions are generated by the gas ionization, these are trapped by the beam potential and drift longitudinally by their thermal energy (0.025 eV) while oscillating radially along the beam axis.

The effect of the ion lifetime and the degree of neutralization have been previously studied [7,13] without taking into account the longitudinal beam electric field. In that case, the ratio of the electron beam density and the ions density will depend on the ion lifetime and neutralization time by

$$\frac{n_i}{n_b} = \frac{t}{\tau}, \tag{2}$$

where t is the ion lifetime.

The ion lifetime in the beamline will be defined by the length of the drift region [8]. In a 1 m drift, the average H_2^+ ion lifetime created along the beam axis is $t_d = 320$ μs. Equation (2) shows the importance of t_d. If the neutralization time is bigger than the ion drift time, the beam neutralization will be negligible because the ion flux losses will overcome the production rate of Eq. (1).

To calculate the electrostatic potential experienced by secondary ions along the beamline at their point of creation and their eventual destination. It is first necessary to determine the beam radius $a(z)$. This can be accomplished by performing the electron beam dynamics calculation using the classic envelope approach and taking into account its perveance [14] or by employing any suitable beam dynamics code. After determining the beam radius $a(z)$, the analytical solution of the electrostatic potential of a dc beam along the line can be calculated using Eq. (3).

$$\phi(r,z) = \begin{cases} \frac{2I}{\beta c 4\pi\epsilon_0}\left(\frac{r^2}{2a^2} - \frac{1}{2} + \ln\left(\frac{a}{b}\right)\right) & 0 < r < a \\ \frac{2I}{\beta c 4\pi\epsilon_0}\ln\left(\frac{r}{b}\right) & a < r < b. \end{cases} \tag{3}$$

Where b is the beam pipe radius, r is the radial position, β is the relativistic factor, and I the beam current. If the beam radius varies slowly in the longitudinal axis, the equation can be obtained to describe the longitudinal profile of the beam potential [13].

For $0 < r < a$, the longitudinal electric field Eq. (4) can be obtained by using the chain rule in the Eq. (3). That is the region where all the ions are created.

$$E_z = -\frac{\partial\phi}{\partial z} = -\frac{\partial\phi}{\partial a}\frac{\partial a}{\partial z}. \tag{4}$$

The longitudinal electric field acting on the ions is proportional to the slope of the beam radius. A positive slope for a divergent beam and the electric field will pull the secondary ions toward the source.

$$\frac{\partial\phi}{\partial a} = \frac{2I}{\beta c 4\pi\epsilon_0}\left(-\frac{r^2}{a^3} + \frac{1}{a}\right) \tag{5}$$

For nonparallel beams, the longitudinal energy gain for a particle of charge q under the beam potential is $q\Delta\phi_z$ using Eq. (3), where a_1 and a_2 are the initial and final beam radius in a beamline, respectively.

$$U = q\Delta\phi_z = \frac{2qI}{\beta c 4\pi\epsilon_0}\ln\left(\frac{a_1}{a_2}\right) \tag{6}$$

Assuming the ion initial velocity as $v_0 = 0$, the final average velocity is $\langle v\rangle = \sqrt{\frac{2q\Delta\phi_z}{m}}$. When the beam is divergent or convergent along the line, it is possible to infer that as the difference between the initial and final beam radius increases [Eq. (7)], the longitudinal velocity (energy) of the secondary ions grows; therefore, its lifetime within the beamline decreases.

$$\langle v\rangle = \sqrt{\frac{qI}{m\beta c\pi\epsilon_0}\ln\left(\frac{a_1}{a_2}\right)}. \tag{7}$$

This new average velocity sets a new limit for the neutralization time where the ions leave the system longitudinally. As an example using Eq. (7) for a divergent beam of 100 keV energy and 10 mA, the average velocity of the ions increases more than 20 times the speed corresponding to its thermal velocity for a change in radius of 10%. This limits the ion density in Eq. (2). The following section studies how this is affected by the neutralization itself.

III. NEUTRALIZATION BEAM ENVELOPE DEPENDENCY

Previous studies [5,6] have extensively studied the secondary ion radial dynamics, showing that the initial particle position and energy determine the maximum radial oscillation of ions and its impact on neutralization. This work examines two different scenarios in which the beam radius changes along the beamline, to understand how this affects the process of clearing ions. In the first scenario, the beam diverges, while in the second scenario, the beam converges to a point within the line. For all cases examined, the electron beam has initial conditions of 100 keV energy, 10 mA current, and a 2 mm radius. Also, the grounded beampipe radius is set to 30 mm.

TABLE I. Secondary ion losses into the two longitudinal boundaries of the beamline (normalized) for different initial beam divergence.

Initial beam divergent α	$z = 0$ m % losses	$z = 0.8$ m % losses
0	0.53	0.47
−10	0.69	0.31
−15	0.74	0.26

A. Divergent beam

After being produced by the source, the beam typically diverges until it reaches the first focusing element. In this scenario, the radius of the beam increases, and the longitudinal gradient defined by Eq. (4) indicates that ions produced in this region are drawn back to the source, where they will later be accelerated by the particle source electric fields.

For the case studied, the system is a 0.8 m drift and the beam parameter α that determines the electron beam divergence ranges between 0 and −15 to avoid beam losses at the beampipe. Without neutralization, and for $\alpha = -15$, the system produces an average beam voltage of 2.3 V. This is sufficient to trap the secondary ions, and due to the beam divergence, all the ions will be drawn to the source and its lifetime in the beamline decreases per Eq. (7).

To study the neutralization dynamics, the residual gas pressure is set to $P_0 = 5 \times 10^{-7}$ mbar where the system reaches an average neutralization level of 50% after reaching steady state and there are no ion radial losses. This pressure level can be considered high in many electron guns.

Once the neutralization reaches steady state, the results of Table I represent the normalized secondary ion losses in the boundaries at the start and the end of the beamline for a series of initial beam divergence values.

The neutralization level is defined as

$$\eta(z) = 1 - \frac{\phi(z)}{\phi_0(z)}, \tag{8}$$

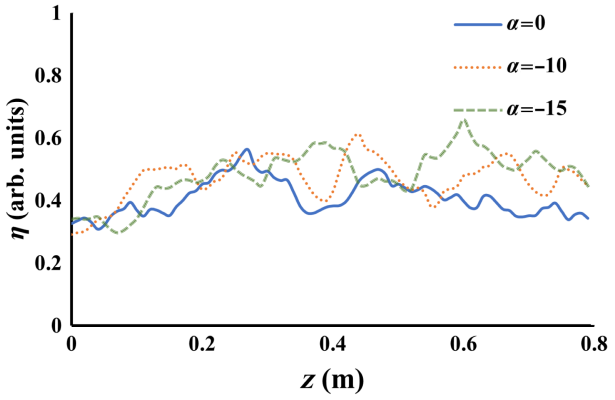

FIG. 1. Neutralization along the line using a 10 mA beam with three different divergence Twiss parameters α.

where $\phi_0(z)$ is the electrostatic potential without compensation. Figure 1 shows the final neutralization level along the beamline for three different α values, where it is clear that it does not change dramatically even when the secondary ion and beam dynamics are not the same.

To explain this, the beamline volume is segmented into differential sections (represented by the mesh in the computer code with a transverse area A). This is done to apply the continuity equation, as shown in Eq. (9) specifically for the secondary ions. Here, the local ion density, denoted as n_i, is determined by the ion current density on the longitudinal faces $J_{\text{ions}}(z)$, and the second term is the creation rate of the ions inside the volume from Eq. (1). dJ_{ions} is the difference in the current density of ions entering and leaving the volume due to the longitudinal electric field determined by Eq. (4).

$$\frac{\partial n_i}{\partial t} A dz = \frac{J_{\text{ions}}(z+dz) - J_{\text{ions}}(z)}{e} + \frac{n_b}{\tau} A dZ = \frac{n_b}{\tau} A dZ - \frac{dJ_{\text{ions}}}{e}. \tag{9}$$

In the steady state, a self-consistent solution emerges, where the ion flux directed toward the beam source stabilizes and therefore dJ_{ions} close to zero. Only the generated ions within the differential volume have a notable contribution. If the local potential increases then dJ_{ions} will also increase again. Consequently, in certain segments of the beamline, the longitudinal electric field tends to level off, approaching the case of $\alpha = 0$, where dJ_{ions} is determined by the ions drifting away from the volume just by its thermal energy. Other studies have shown the electric potential oscillation due to neutralization along the line that impacts the ion velocity distribution [15].

Due to the longitudinal ion losses, Eq. (9) always gives a smaller n_i in comparison to Eq. (1). Marking the difference in comparison to the case where the longitudinal component is neglected.

The extreme case is when there is an external electric field clearing the ions and increasing to a maximum dJ_{ions} results in a negligible neutralization even for high pressures.

In the case of divergent beams to prevent source ion back bombardment, it is necessary to suppress the ion losses in the $z = 0$ boundary from Table I. A solution that has been successfully implemented is to apply a positive bias voltage to the anode. This positive potential effectively repels beamline ions away from the electron source longitudinal accelerating electric field [1]. This solution creates a trap that enhances the neutralization factor of the beam [4], and its implications for beam dynamics must be carefully considered.

B. Convergent beam

Another case to be studied is when the beam has a focal point inside the drift section. This configuration can be

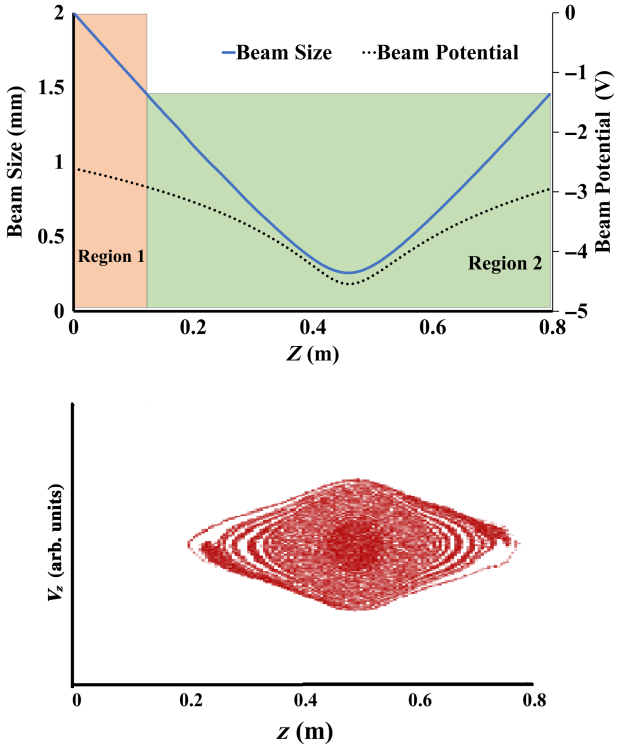

FIG. 2. Beam envelope and potential along the beamline. Bottom: expected ion velocity distribution around the focal point in one dimension without neutralization. Secondary ions originating in region 2 are trapped, while those in region 1 are not confined.

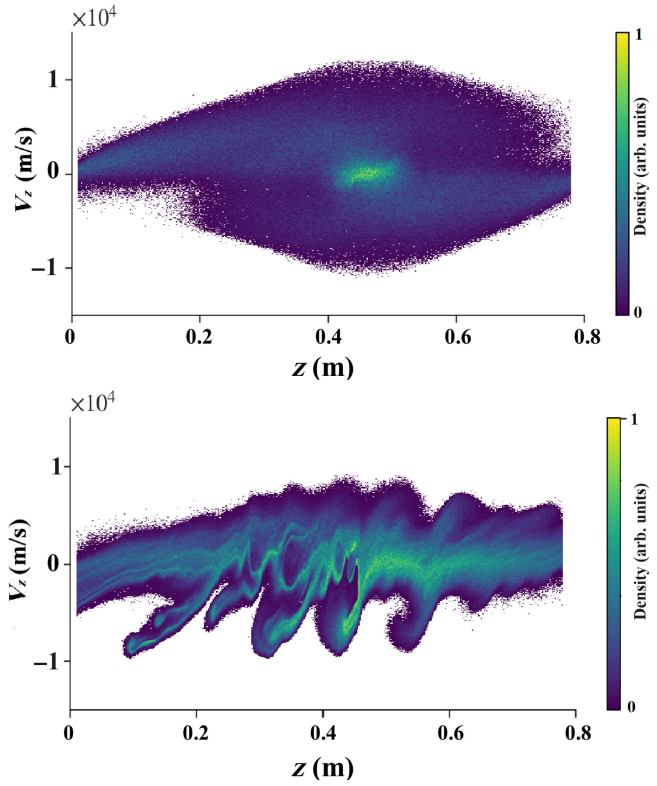

FIG. 3. Ion distribution velocity. Top: in the neutralization early stage. Bottom: once the beam is neutralized.

achieved in an electron gun producing a beam with a focal point upstream of the first focusing element.

Figure 2 illustrates the beam radius alongside the electrostatic potential. For this example, the beam has the same initial conditions as in the previous case, but with a positive α to make the beam converge to a size of 0.2 mm before diverging again to achieve a size of 1.5 mm at the end of the beamline. The generated secondary ions converge toward the beam focal point within the drift. The behavior of the ions can be computed using Eq. (3). The results are shown in Fig. 2, where the ion dynamics is similar to the radial movement in which the trapped ions rotate around the beam potential well [6,7].

The asymmetry generated by the longitudinal change in the beam radius creates two regions. In region 2 (Fig. 2), the initial beam size is below 2 mm, and all the ions generated within are trapped and rotated around the focal point. In region 1 where the beam size is bigger than 1.5 mm, the generated ions are driven to the focal point, but once there, the ions have enough kinetic energy to overcome the potential well and continue to the boundary at $z = 0.8$ m.

Figure 3 shows the velocity distribution of the ions by taking into account the neutralization effect in IBsimu. In the first moments of neutralization, the ions rotate around the focal point as expected, defining a capture volume where the beam size is less than 1.5 mm. Particles outside region 2 possess sufficient kinetic energy to exit the system.

If the neutralization is negligible, the volume where the ions are created and escape back to the source can be considered fixed. Only the particles created outside the capture volume determined by the beam radius above 1.5 mm escape from the system resulting in negligible source ion back bombardment.

When the pressure is high enough to trigger neutralization, the previously described ion dynamics reduce the

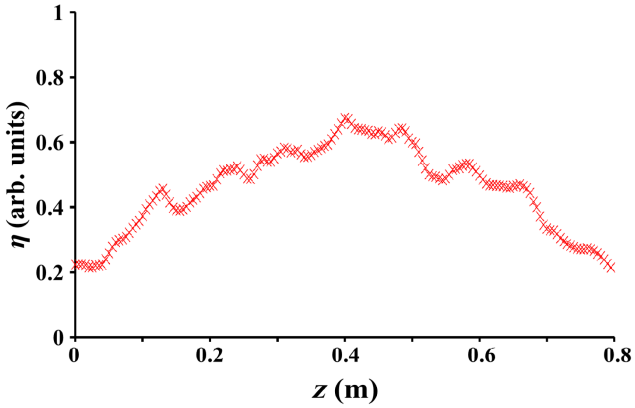

FIG. 4. Neutralization level along the beamline after the steady state is reached.

beam potential decreasing the longitudinal differences along the beamline. This trend reduces the capture volume until the steady state is reached, and the ions escape from regions where they were previously longitudinally confined, as shown in Fig. 3. The potential reduction ends in a nonlinear neutralization (Fig. 4), due to the ions concentration in the beam focal point.

To reduce the ion losses in the boundary $z = 0$ (which can be interpreted as ion back bombardment), it is recommended to position the capture volume outside the range of the electron gun electrostatic potential to ensure the ion oscillation along the electron beam focal point. Additionally, the size of the beam at the end of the beamline relative to its size at the start needs to be smaller to enhance the ion mobility in the positive direction.

IV. SOLENOID MAGNET

To manage beam divergence in the low energy beamline, a common approach is employing a solenoid. The solenoid magnetic fields also impact the dynamics of the secondary ions. In the specific case under study, the beam exhibits divergence upstream of the solenoid ($\alpha = -10$) and subsequently gets focused with the opposite slope ($\alpha = 10$). The solenoid length is 0.2 m and its strength is $\int B^2 dz = 0.16$ mT^2 m. Studies about Gabor lenses have revealed that ion accumulation, where the space charge gets neutralized within the solenoid, typically occurs in magnetic fields stronger than the one employed in this study [16].

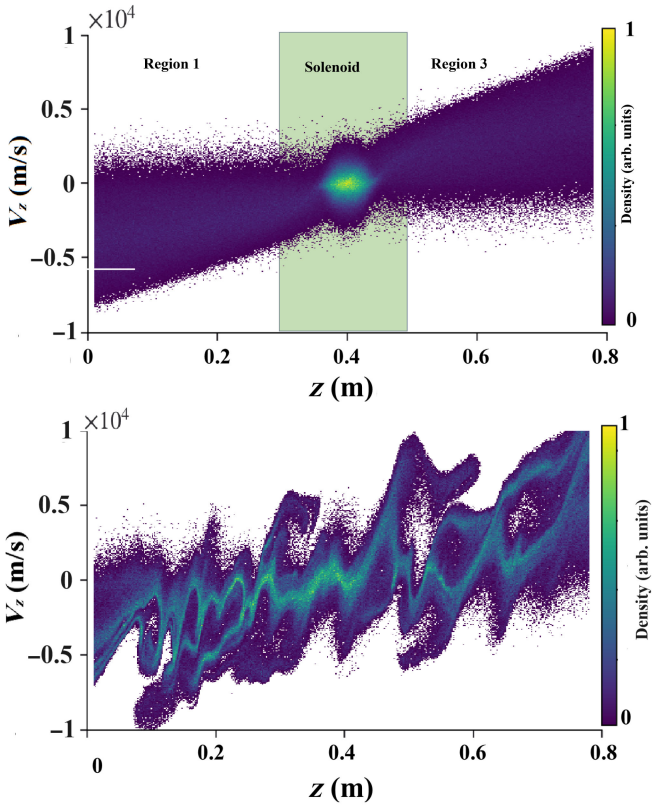

FIG. 5. Ion velocity distribution for the solenoid. Top: in the neutralization early stage. Bottom: once the beam is neutralized.

As illustrated in Fig. 5, the solenoid effectively segments the beamline into three distinct sections. The ions in the upstream section naturally gravitate toward the source. The ions generated downstream of the solenoid are directed further downstream into the accelerator. The region inside the solenoid tends to accumulate a higher secondary particle count as a consequence of the magnetic field. The average neutralization level in the beamline is 35%.

Similar to the previous case, this configuration tends to decrease the overall potential as the ions accumulate along the beamline. However, the longitudinal potential difference along the beamline is not fully eliminated. The ions persistently adhere to their trajectories, either moving toward the source or advancing toward the subsequent accelerator segments. Due to the larger beam size and ion density inside the solenoid, the middle section of the system exhibits the lowest beam potential, this effect increases the longitudinal electric field, enhancing the ion mobility inside the solenoid field and decreasing the ion concentration in the middle of the beamline.

V. LONGITUDINAL BOUNDARY CONDITIONS

To investigate the impact of the longitudinal boundary conditions on the neutralization level, three conditions are set as follows: the first condition where both boundaries are open, the second where $\phi(z = 0) = 0$, and the third called "closed" with $\phi(z = 0) = \phi(z = 0.8) = 0$, this case can be achieved, for example, when a diagnostic device like an emittance measuring device or a Faraday cup is inserted into the beamline [17,18].

For initial beam divergence, $\alpha = 0$. Figure 6 shows the result of the different levels of neutralization for the three boundary conditions along the beamline after the steady state is reached.

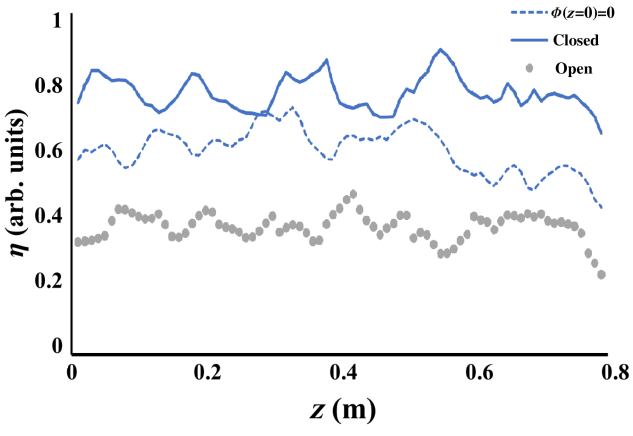

FIG. 6. Neutralization level for the three longitudinal boundary conditions where the electrostatic potential is set to zero at one or both ends (closed) and where no bias is applied (open).

How the neutralization is connected to the longitudinal boundary conditions is related to the ion lifetime and whether the ions can leave the system longitudinally. As Eqs. (2) and (9) state, the level of neutralization reached within a volume depends on the ion creation rate and flux into the volume. In the closed case, the ions can only escape radially and the conditions for the full neutralization obey previous works' predictions [6,7].

For open boundaries, the ions drift to both ends of the beamline and then escape. Once the potential is set $\phi(z=0)=0$, the ions traveling backward to $z=0$ are forced to oscillate at the end of the beamline, traveling longer around the system to escape at $z=0.8$ m. For this case, the neutralization is higher than for open boundaries due to the asymmetry caused by more particles traveling from left to right. This enhances the first term of Eq. (9) leaving the neutralization level for the open boundaries at 50% of the closed case. Considering this factor, when measuring beam properties is essential, the measurement devices can alter the boundary conditions.

VI. CONCLUSIONS

The longitudinal dynamics of secondary ions are influenced by the beam potential, which can either pull ions toward or push them away from the electron source. To understand where the ions will end, we can use the analytical solution for a line of charge. This helps us calculate how ions move, especially in situations where the beam neutralization is negligible.

When there are no external fields in the beamline, the neutralization reduces the beam potential, and as a result, the differences in potential along its longitudinal length tend to diminish. It is important to note that this reduction does not always bring the neutralization level to 100% and the ions longitudinal dynamics is mainly influenced by the drift resulting from their thermal energy.

When the beam starts diverging right from the source, all ions generated upstream of the first focusing element get pulled back to the source, resulting in ion back bombardment. However, this problem can be decreased or canceled by biasing the extraction system. If a solenoid is included in the system, it stops the cancellation of the longitudinal potential difference and the ions continue to be trapped by the beam electrostatic potential.

If the goal is to prevent ion back bombardment without implementing external fields in the beamline next to the electron gun, one potential solution is to produce a convergent beam from the source to deflect ions away, creating an ion capture volume. However, it is important to note that the longitudinal beam potential well in this configuration tends to decrease as secondary ions fill it. As a result, the level of neutralization along the beamline is not uniform and needs to be considered because many studies in beam dynamics often assume a constant level of neutralization along the whole beamline.

The longitudinal boundary conditions at the beamline play a crucial role in determining the level of neutralization that can be attained. With the same residual gas pressure, these conditions can range from full neutralization to less than 50%.

ACKNOWLEDGMENTS

Part of this work was supported by the Universidad Autonoma de Sinaloa (Grant No. PRO A1 022) and by CONACYT (Grant No. CF-2019/2042).

[1] J. Grames, R. Suleiman, P. A. Adderley, J. Clark, J. Hansknecht, D. Machie, M. Poelker, and M. L. Stutzman, Charge and fluence lifetime measurements of a dc high voltage gaas photogun at high average current, Phys. Rev. ST Accel. Beams **14**, 043501 (2011).

[2] C. Sinclair, Recent advances in polarized electron sources, in *Proceedings of the 18th Particle Accelerator Conference, New York, 1999* (IEEE, New York, 1999), pp. 65–69.

[3] O. Rahman, E. Wang, I. Ben-Zvi, J. Biswas, and J. Skaritka, Increasing charge lifetime in dc polarized electron guns by offsetting the anode, Phys. Rev. Accel. Beams **22**, 083401 (2019).

[4] C. Hernandez-Garcia, P. Adderley, B. Bullard, J. Benesch, J. Grames, J. Gubeli, F. Hannon, J. Hansknecht, J. Jordan, R. Kazimi, G. A. Krafft, M. A. Mamun, M. Poelker, M. L. Stutzman, R. Suleiman, M. Tiefenback, Y. Wang, S. Zhang, H. Baumgart, G. Palacios-Serrano, S. Wijethunga, J. Yoskowitz, C. A. Valerio Lizarraga, R. Montoya Soto, and A. Canales Ramos, Compact −300 kV dc inverted insulator photogun with biased anode and alkali-antimonide photocathode, Phys. Rev. Accel. Beams **22**, 113401 (2019).

[5] K. Aulenbacher, C. Nachtigall, H. Andresen, J. Bermuth, T. Dombo, P. Drescher, H. Euteneuer, H. Fischer, D. Harrach, P. Hartmann, J. Hoffmann, P. Jennewein, K. Kaiser, S. Köbis, H. Kreidel, J. Langbein, M. Petri, S. Plützer, E. Reichert, M. Schemies, H.-J. Schöpe, K.-H. Steffens, M. Steigerwald, H. Trautner, and T. Weis, The MAMI source of polarized electrons, Nucl. Instrum. Methods Phys. Res., Sect. A **391**, 498 (1997).

[6] I. A. Soloshenko, Space charge compensation of technological ion beams, in *Proceedings of the 18th International Symposium on Discharges and Electrical Insulation in Vacuum (Cat. No.98CH36073), Eindhoven, Netherlands*, ISDEIV (1998), Vol. 2, pp. 675–678, 10.1109/DEIV.1998.738839.

[7] A. BenIsmail, R. Duperrier, D. Uriot, and N. Pichoff, Space charge compensation studies of hydrogen ion beams in a drift section, Phys. Rev. ST Accel. Beams **10**, 070101 (2007).

[8] R. Becker and M. Kleinod, Space charge compensation of electron beams by thermal ions and the production of highly charged ions in EBIS and EBIT, Rev. Sci. Instrum. **65**, 1063 (1994).

[9] C. A. Valerio-Lizarraga, I. Leon-Monzon, and R. Scrivens, Negative ion beam space charge compensation by

residual gas, Phys. Rev. ST Accel. Beams **18**, 080101 (2015).

[10] N. Chauvin, Simulation and measurements in high intensity LEBT with space charge compensation, in *Proceedings of HB2012, Beijing, China* (2012), Vol. 2, pp. 508–510, https://accelconf.web.cern.ch/HB2012/papers/tho3a03.pdf.

[11] T. Kalvas *et al.*, IBSIMU: A three-dimensional simulation software for charged particle optics, Rev. Sci. Instrum. **81**, 02B703 (2010).

[12] J. Yoskowitz, Simulating electron impact ionization using a generalparticle tracer (GPT) custom element, in *Proceedings of the 12th International Particle Accelerator Conference, IPAC-2021, Campinas, SP, Brazil* (JACoW, Geneva, Switzerland, 2021), pp. 65–69.

[13] E. Pozdeyev, Ion trapping and cathode bombardment by trapped ions in dc photoguns, Phys. Rev. ST Accel. Beams **10**, 083501 (2007).

[14] J.-F. A. A. Perrin and T. Muetze, Travel User Manual.

[15] I. A. Soloshenko, Physics of ion beam plasma and problems of intensive ion beam transportation (invited) (abstract), Rev. Sci. Instrum. **67**, 1270 (1996).

[16] J. Palkovic, F. Mills, C. Schmidt, and D. Young, Gabor lens focusing of a negative ion beam, in *Proceedings of the 1989 Particle Accelerator Conference, Chicago, IL* (IEEE, New York, 1989), Vol. 1, pp. 304–306.

[17] A. Laxdal, F. Ames, B. R., S. R. Koscielniak, M. D., W. Rawnsley, and P. Vincent, High power Allison scanner for electrons, in *Proceedings of the Beam Instrumentation Workshop, BIW2012, Newport News, VA* (JACoW, Geneva, Switzerland, 2012), pp. 133–135.

[18] R. F. Schneider, J. R. Smith, and M. J. Rhee, Emittance meter for time resolved electron beam propagation studies, Rev. Sci. Instrum. **59**, 186 (1988).